



Comparison of hollow fiber module designs in membrane distillation process employed lumen-side and shell-side feed

Dan Qu*, Tuantuan Zhou, Weifang Ma, Zhuoqun Peng, Zhi Li, Mengting Qin

College of Environmental Science and Engineering, Beijing Forestry University, Beijing 100083, China, Tel. +86 13811836963; email: qudana@163.com (D. Qu), Tel. +86 18611267178; email: 1348583028@qq.com (T. Zhou), Tel. +86 13911709575; email: mpeggy@163.com (W. Ma), Tel. +86 18811371985; email: 2318103922@qq.com (Z. Peng), Tel. +86 18911740436; email: 565222817@qq.com (Z. Li), Tel. +86 18811371853; email: 907358980@qq.com (M. Qin)

Received 31 December 2014; Accepted 3 May 2015

ABSTRACT

In the present work, randomly packed, curly fiber, spacer scattered, and spacer knitted modules were fabricated and their performance in direct contact membrane distillation employed lumen-side feed and shell-side feed was investigated, respectively. Experimental results showed that the flux of different module configurations in shell-side feed operations were lower than that in lumen-side feed operations. Modified modules showed higher flux compared with randomly packed module and the spacer knitted module had the best performance with 51.8% enhancement at 328 K in lumen-side feed performance. The module flux increased as the feed flow rate increased, and all the modified modules showed relative high flux even at a low feed flow rate, which confirmed the fluid improvement caused by the spacers or wavy geometries. The overall heat transfer coefficient of modules ranged from 704 to 1,961 W/(m² K) in lumen-side feed operations, while that was lower to be 425–645 W/(m² K) in shell-side feed operations. In addition, higher heat transfer coefficients and temperature polarization coefficient were observed with modified module configurations. The sodium chloride tracer response technique was used to reveal the shell-side flow pattern and distribution for various module designs. Results showed that the modified module configurations can provide a better flow distribution in shell side with longer residence time and smaller variance, thus higher thermal efficiency and flux could be accomplished.

Keywords: Hollow fiber module; Modification; Membrane distillation; Shell-side feed; Lumen-side feed; Temperature polarization

1. Introduction

Membrane distillation (MD) is a thermally driven process that vapor transports through non-wetted

hydrophobic pores, where the driving force is the partial vapor pressure difference across the feed and permeate sides. Compared with pressure-driven membrane processes such as reverse osmosis and nanofiltration, the advantages of MD includes: less dependence on the initial feed salinity and

*Corresponding author.

Presented at the 7th International Conference on Challenges in Environmental Science and Engineering (CESE 2014) 12–16 October 2014, Johor Bahru, Malaysia

theoretically 100% salt rejection; low membrane fouling; mild operating conditions and less demanding in membrane's mechanical strength; feasibility to utilize low-grade heat and renewable energy (e.g. waste heat or solar power). Thus, it is a promising technique for water desalination and high concentration wastewater treatment. There are four basic configurations of membrane distillation (MD), including direct contact membrane distillation (DCMD), vacuum membrane distillation, air gap membrane distillation, and sweep gas membrane distillation [1]. And DCMD is the most studied and simple mode among the configurations [2].

Despite many attractive characteristics and lab-scale studies, MD has not been widely implemented in industry [3,4]. One of the main challenges is the flow maldistribution and/or poor hydrodynamics in the membrane module as well as the severe temperature polarization (TP) that compromises module performance [1]. It is well recognized that the module is the core part of membrane processes. The industrial membrane separation requires large areas of membrane surface to be economically and effectively packaged [5]. Properly designed module will result in enhanced productivity, decreased energy consumptions, and long membrane lifespan [6]. So there is an urgent need for the development of proper membrane modules.

Hollow fiber modules are preferable for industrial applications due to their flexibility, larger membrane area per unit volume, and high productivity [1]. Now randomly packed module is widely used in MD [7–11]. However, serious non-ideal flow distribution such as channeling, bypassing was found in the shell side of randomly packed modules, which resulted in less active membrane area, insufficient mixing and local loss of driving force, and hence low heat and mass transfer efficiencies [12]. So many researchers investigated strategies to improve MD performance such as optimizing operation parameters and designing novel modules to improve the flow distribution and alleviate the TP phenomenon.

Some studies have focused on the effect of module size, packing density, and fiber length on the module productivity [13–15]. Yang et al. found that the driving force decreased with the increasing fiber length due to the rapid buildup of thermal boundary layers, which reduced the temperature difference across the membrane and inhibited the mass and heat transfer. A critical length existed which is the operational length to assure sufficient driving force along the fiber to maintain a higher MD efficiency. In addition, the MD coefficient decreased with increasing packing density [15].

Some studies focused on the permeate flux enhancement and TP mitigation by incorporating proper flow alteration aids or modifying fiber geometries to create secondary flows or eddies in the module [12,16–19]. An early exploration on hollow fiber module design by Schneider et al. investigated the effects of module size and modified fiber geometries on the transmembrane flux of the DCMD process. It showed that larger modules could achieve uniform flow more easily than smaller ones and certain hollow fiber arrangements could lead to much higher fluxes than those with straight woven fabric designs [16]. Martinez-diez et al. reported two different separator configurations, open flow and screen separators for flux enhancement in a DCMD module, and found that the screen separator was more efficient due to turbulent flow generation and suppression of TP [17]. In 2008, Teoh et al. investigated different hollow fiber module designs with baffles, spacers, and modified hollow fiber geometries for flux enhancement in the MD process. It was found that the application of window and helical baffles resulted in 20 and 28% flux enhancements, respectively, while hollow fiber configurations with wavy geometries (twisted and braided) enabled the highest flux enhancement to 36% [18].

Besides the DCMD performance, the flow distribution and TP analysis were also investigated in the novel module configurations. Yang et al. applied tracer response tests for the measurement of shell-side flow distribution in different modules (structured straight fibers, curly fibers, central tubing, spacer wrapped and spacer knitted modules), and the results showed that improved fiber geometries or arrangements can provide a better flow distribution, thus much lower pumping energy cost and higher thermal efficiency could be accomplished. A significant flux enhancement from 53 to 92% was found compared to the conventional module and the curly fiber module had the best performance [12]. In another work by Yang et al. low field bench top nuclear magnetic resonance imaging was used to investigate the hydrodynamics in novel hollow fiber modules of randomly packed, spacer knitted, curly and semi-curly fibers. Valuable information including imaging, spatially resolved velocity maps, and probability distributions of velocity were acquired and revealed the existence of reduced stagnant regions and significant transverse flow at varied operating conditions in novel hollow fiber modules. A better overall mixing was shown and hence confirmed their better module performance [19].

All the above reported studies focused on the DCMD process based on shell-side feed operation. However, lumen-side feed is commonly adopted in DCMD process [7–11]. And till now, no report is

found to investigate the DCMD performance of modified module configurations based on lumen-side feed. And there is also lack of knowledge in the difference between shell-side feed and lumen-side feed performance of modified modules.

Therefore, this work attempts to investigate the DCMD performance of different modules on the condition of lumen-side and shell-side feed. Randomly packed, curly fibers, spacer scattered and spacer knitted module were fabricated. The flux and heat transfer analysis of lumen-side and shell-side feed operations were investigated. In addition, the residence time distribution (RTD) based on sodium chloride tracer response were also studied for various modules.

2. Experimental

2.1. Membrane

Polypropylene (PP) hollow fiber membrane (Accurel PP Q3/2, Membrana, Germany) was used and the characteristics are shown in Table 1.

2.2. Hollow fiber modules fabrication

Randomly packed module, curly fibers, spacer scattered and spacer knitted module were fabricated in this study just as seen in Fig. 1(a)–(d). Fig. 1(a) shows a randomly packed module. To create curly fibers, straight hollow fibers were inserted in a wryer net and heated in an oven at 80 °C for 30 min in order to induce a wavy shape on the fibers. And then the wryer net was removed and the curly fibers were got (Fig. 1(b)). For the spacer scattered module (Fig. 1(c)), three pieces of sieve spacer were placed at both the ends and middle of the module to make the fibers scattered and equispaced. The spacer knitted module was shown in Fig. 1(d). PP hollow fibers were knitted into the mesh of the spacer and then packed in the plexiglass tube.

The detailed information of various modules is shown in Table 2. Each module was prepared by loading 60 hollow fiber membranes into a plexiglass tube with effective length of 180 mm. The effective membrane area was 0.029 m². The packing density was

15%. The ends of the module were sealed by epoxy resin and cured for 48 h at room temperature.

2.3. Module performance evaluation

The DCMD performance of modules employing lumen-side feed and shell-side feed was investigated on the condition of different feed temperature (308–328 K) and feed flow rate (1.0–2.5 L/min). A laboratory scale DCMD setup, which is shown in our previous work, was used for the performance evaluation [11]. One percentage of sodium chloride solution was used as the feed solution while the permeate solution was deionized water. The feed and permeate solutions were pumped countercurrently through the hollow fibers.

2.4. Tracer response tests

The tracer response tests were conducted using the same DCMD setup to investigate the shell-side flow distribution. Fig. 2 schematically shows the location of tracer injection and effluent concentration monitors. At room temperature, deionized water was pumped at 1.0 L/min into the shell side of the modules as the feed solution (blank background solution) a pulse input of sodium chloride was injected at the feed inlet. The tracer response signal was measured using a conductivity meter ($\pm 0.1 \mu\text{S}/\text{cm}$) installed at the exit of the effluent. The effluent signals were recorded via a data-acquisition system. To obtain reproductive and comparable results, the tracer tests for each module were repeated 10 times under constant operating conditions.

3. Theory

3.1. Heat transfer and TP coefficient analysis

TP commonly exists in MD processes, so the wall temperatures may be significantly different from the bulk temperatures [1,20]. TP coefficient (TPC, τ) can be used to quantify the TP effect. TPC is a function of both the feed and permeate boundary layers, which are influenced by the fluid properties, operating parameters, and hydrodynamic conditions. It is defined as Eq. (1).

Table 1
Characteristics of PP hollow fiber membranes

Inner diameter	Outer diameter	Porosity	Average pore size	Thickness	LEPw
0.7 mm	1.0 mm	80%	0.38 μm	0.15 mm	440 kPa

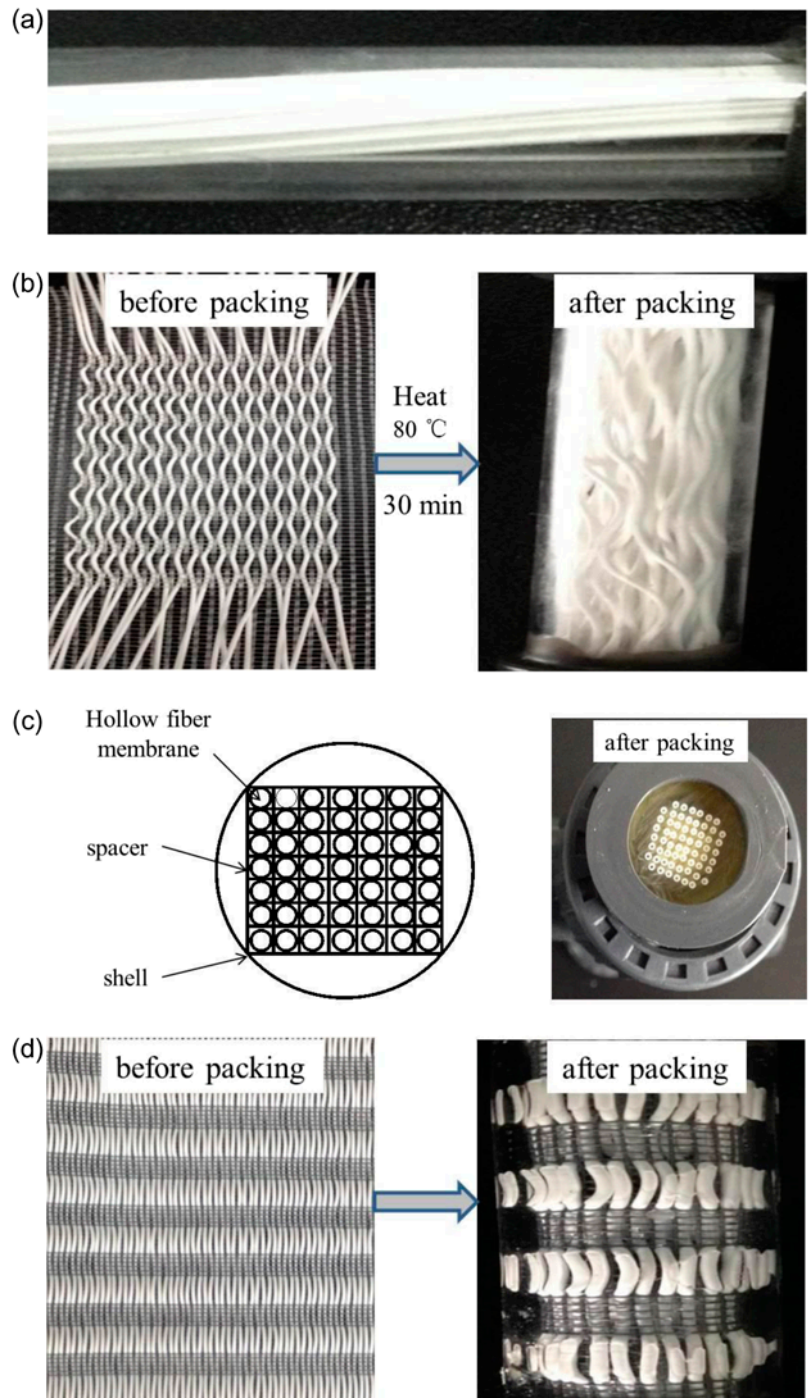


Fig. 1. Module designs and fabrication: (a) randomly packed module; (b) curly fiber module; (c) spacer scattered module; (d) spacer knitted module.

$$TPC = \frac{T_{fm} - T_{pm}}{T_f - T_p} \quad (1)$$

where T_f and T_p (K) is the bulk temperature of the feed and permeate, respectively. And the T_{fm} and T_{pm}

(K) is the temperature at the membrane surface of the feed and permeate, respectively.

To solve for the TPC, it is necessary to determine the relation between the heat and mass transfer in the direction from the hot feed to cold permeate. Following modeling and assumptions are applied.

Table 2
Characteristics of hollow fiber membrane modules

Membrane module configurations	Module housing diameter (mm)	Membrane (area/m ²)	Effective fiber length (mm)	No. of fibers, <i>n</i>	Packing density (%)
Randomly packed module	20	0.029	180	60	15
Curly fiber module	20	0.029	180	60	15
Spacer scattered module	20	0.029	180	60	15
Spacer knitted module	20	0.029	150	60	15

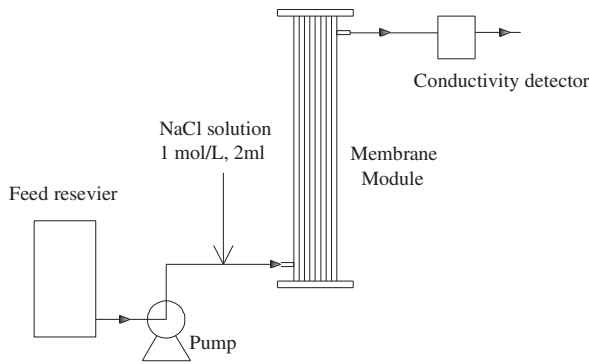


Fig. 2. Schematic diagram of tracer response experiment.

- (1) The permeate flux N (L/(m² h)) can be expressed in terms of the transmembrane temperature difference, when the pure water was used as feed [20].

$$N = C \frac{dP}{dT} \Big|_{T_m} (T_{fm} - T_{pm}) \quad (2)$$

where C is the mass transfer coefficient (kg/(m² h kPa)), T_m is the membrane temperature (K), and can be estimated by $(T_f + T_p)/2$. dP/dT is the vapor pressure gradient, and can be calculated based on the Clausius-Clapeyron equation, as seen in Eq. (3).

$$\frac{dP}{dT} \Big|_{T_m} = \frac{P\lambda M}{RT^2} \Big|_{T_m} \quad (3)$$

where λ is the latent heat of vaporization (kJ/kg), M is the molecular weight of water ($M = 18$ g/mol), R is the gas constant ($R = 8.314$ J/(mol K)), and P (kPa) is saturated vapor pressure and can be obtained from Antoine equation (Eq. (4)) [21].

$$\lg P = A - \frac{B}{C + t} \quad (4)$$

where P (mmHg) was the water vapor pressure. T (°C) was the temperature. A , B , C is the constant with values of 8.07, 1,730.63, 233.43, respectively.

- (2) The heat transferred across the feed/permeate boundary layers is equal to the overall heat transfer across the membrane [20]. Eqs. (5) and (6) define the heat transferred across the feed/permeate boundary layers, respectively. And Eq. (7) defines the heat transported across the membrane, which consists of conductive heat through membrane q_c (W/m²) and the latent heat transfer contributing to the water vapor flux q_v (W/m²):

$$q_f = h_f(T_f - T_{fm}) \quad (5)$$

$$q_p = h_p(T_{pm} - T_p) \quad (6)$$

$$\begin{aligned} q_m &= q_c + q_v = \left(\frac{k_m}{\delta_m} \right) (T_{fm} - T_{pm}) + N\lambda \\ &= \left(\frac{k_m}{\delta_m} \right) + \lambda C \frac{dP}{dT} \Big|_{T_m} (T_{fm} - T_{pm}) = h_m(T_{fm} - T_{pm}) \end{aligned} \quad (7)$$

where h_f and h_p (W/(m² K)) refers to the heat transfer coefficient for the feed and permeate sides, respectively; h_m (W/(m² K)) is the efficient heat transfer coefficient based on the transmembrane temperature difference, δ_m (m) is the wall thickness of membrane, and k_m (W/(m K)) is the overall thermal conductivity of the membrane. The effective conductivity k_m can be estimated from the vapor and solid phase thermal conductivities, just as shown in Eq. (8).

$$k_m = (1 - \varepsilon)k_s + \varepsilon k_v \quad (8)$$

where ε is the membrane porosity (%), and k_s and k_v are thermal conductivities for solid and gases in the pores, respectively. In this study, k_s and k_v is 0.18 and

0.026 W/(m K). The δ_m of the used PP hollow fiber membrane is 0.15 mm, so the k_m/δ_m value is 366.5 W/(m² K).

The following equations can be yield by combining Eqs. (5)–(7). H (W/(m² K)) is the overall boundary layer heat transfer coefficient and equal to $1/(1/h_f + 1/h_p)$.

$$\frac{\Delta T}{N\lambda} = \frac{1}{dP/dT} \frac{1}{\lambda C} \left(1 + \frac{k_m/\delta_m}{h} \right) + \frac{1}{H} \quad (9)$$

Parameter such as ΔT , N , λ , k_m/δ_m , as well as the dP/dT are obtainable. The unknown parameters H and C can be calculated from the intercept and the slope by plotting $\frac{\Delta T}{N\lambda}$ and $\frac{1}{dP/dT}$ [20]. And TPC can also be calculated.

3.3. Residence time distribution (RTD)

The RTD can be used to assess the degree of mixing and flow patterns within many kinds of reactors. It is a common practice to use the probability function $E(t)$ to describe the distribution of residence times, which can be evaluated by dividing temporal variation of tracer concentration ($C(t)$) in the membrane shell side by the total mass of tracer injected in the feed ($\int_0^\infty C(t) dt$), just as shown in Eq. (10) [22].

$$E(t) = \frac{C(t)}{\int_0^\infty C(t) dt} \quad (10)$$

In the RTD tests, mean residence time (t_m , s) is a key parameter to describe the fluid flow in the shell. According to the RTD curves, the mean residence time can be calculated based on Eq. (11).

$$t_m = \int_0^\infty tE(t) dt \quad (11)$$

The theoretical residence time t , known as holdup time, is equal to the actual vessel volume V divided by the fluid flow rate Q_0 . In a hollow fiber MD module the difference between t and t_m shows the mixture of fluid in the shell, i.e. a larger deviation might indicate a longer contact time and hence, more effective heat transferred across the membrane [12].

The spread in residence time is characterized by the variance σ^2 and it can be calculated based on Eq. (12). A larger variance value indicates a wider spread of residence time or more deviation from the uniform flow pattern [22].

$$\sigma^2 = \int_0^\infty E(t)(t - t_m)^2 dt \quad (12)$$

4. Results and discussion

4.1. DCMD performance of different module configurations

Fig. 3 shows the permeate flux as a function of feed temperature (T_f) for different module configurations. The solid line represents the permeate flux when the feed were pumped through the lumen side (lumen-side feed), while the dashed line represents the permeate flux when the feed were pumped through the shell side (shell-side feed). Compared with randomly packed module, all the three designed modules showed improved flux both on the condition of lumen-side and shell-side feed. The greatest flux enhancement of 51.8% was observed at 328 K with the spacer knitted module employed lumen-side feed. While the flux enhancement of 30.2 and 38.8% was observed at 328 K with curly fibers and spacer scattered modules, respectively (lumen side feed). It is known that the hydrophobic materials are repelled by water and often cluster together in water which might lead to a lower effective membrane surface area [18]. The spacers and curly fibers can directly prevent the fibers from sticking together, thus the membranes can be able to efficiently function in aqueous solutions. And the spacers and un-straight geometry of hollow fibers may also act as a static mixer for the shell-side to facilitate a meandering fluid flow, and thereby achieve a well-mixed condition (discussed in

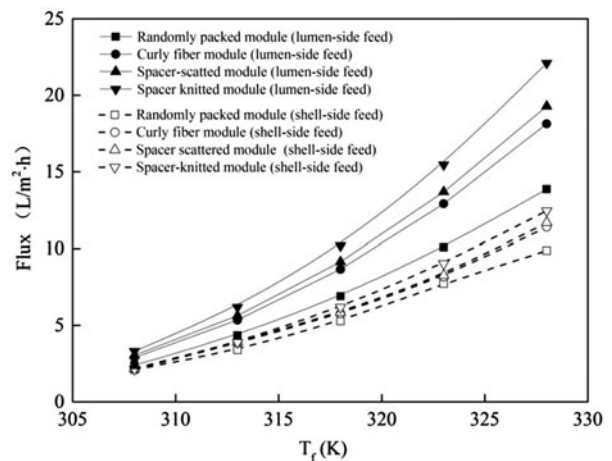


Fig. 3. Fluxes of different module configurations in DCMD employed lumen-side and shell-side feed ($Q_f = Q_p = 2.5$ L/min, $T_f = 308$ – 328 K, $T_p = 298$ K).

Section 4.4), which can help to mitigate the TP and favors for heat transfer (discussed in Section 4.3).

It can be also observed from Fig. 3 that the flux of modules employed lumen-side feed was higher than that of modules employed in shell-side feed. For example, the flux of spacer knitted module ranged from 3.9 to 20.1 L/m² h in lumen-side feed operation; while it was lower to be 2.4–12.4 L/m² h in shell-side feed operation. In this study, the Q_f and Q_p was both 2.5 L/min, so the flow velocity of lumen side (1.86 m/s) was much higher than that of shell side (0.16 m/s) due to their different flow areas. Normally, the TP in the feed side was higher than that in the permeate side. A higher feed recirculating velocity can help to reduce the thickness of the hot boundary layer adjacent to membrane surface and maximize the driving force [12,23]. Furthermore, serious channeling, bypassing, or dead zones in shell-side were avoided in feed when the feed was pumped through the lumen side. A more effective contact of hot feed and membrane resulted in a higher permeate flux which was confirmed by Fig. 3.

Feed velocity is a significant influencing parameters on the permeate flux. As discussed previously, the feed flow velocity is much higher in the lumen side especially on the condition of low module packing density with thin hollow fibers. So when the feed is pumped through the shell side, increased pumping energy is required to provide a higher velocity to obtain high flux. It is not an economical way to improve flux, so DCMD employed lumen-side feed in recommend.

4.2. Effect of feed flow rate on permeate flux for different module configurations

The permeate flux at different feed flow rate both on the condition of shell-side feed (dashed line) and lumen-side feed (solid line) is shown in Fig. 4. When the Q_f increased from 1.0 to 2.5 L/min, the V_f was different in the shell and lumen side. When the feed was pumped through the shell side, the $V_{f,shell}$ was in a lower range of 0.06–0.15 m/s, and the $V_{p,lumen}$ was 0.72 m/s. And when the feed was pumped through the lumen side, at the same flow rate (Q_f , L/min), the $V_{f,lumen}$ increased to 0.7–1.8 m/s, and $V_{p,shell}$ was 0.06 m/s. The feed velocity played an important role in the DCMD process, so the module flux on the condition of lumen-side feed was higher due to higher feed flow velocity. The flux_{lumen-side feed} was observed to be 5.3–9.8 L/m² h, while the flux_{shell-side feed} was only 3.6–5.5 L/m² h.

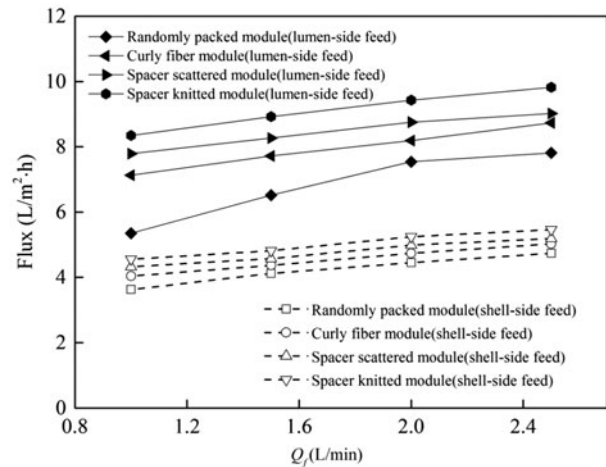


Fig. 4. DCMD performance of different module configurations at different feed temperature ($T_f = 318$ K, $T_p = 298$ K, $Q_f: 1.0$ – 2.5 L/min; $Q_p: 1.0$ L/min).

The curly fiber, spacer scattered and spacer knitted module showed relatively higher flux than randomly packed module both on the condition of shell-side feed and lumen-side feed at different Q_f . And all the modified module configurations showed relative high flux even at a low Q_f , which confirms the fluid improvement caused by the spacers or wavy geometries, and results in a higher flux even at low feed flow rate. The flux enhancement of 15–33% on the condition of shell-side feed was observed, while a more significant improvement of 25–55% on the condition of lumen-side feed over the randomly packed module was observed due to a more efficient heat transfer in lumen side.

4.3. Temperature polarization coefficient and heat transfer analysis

Base on Eq. (9), the overall heat transfer coefficient H can be calculated from the intercept by plotting $\frac{\Delta T}{N\Delta}$ and $\frac{1}{dP/dT}$. The overall heat transfer coefficients of different modules both on the condition of lumen-side feed and shell-side feed are summarized in Table 3. It can be seen from Table 3 that the overall heat transfer coefficients of designed modules were all higher than that of randomly packed module. Furthermore, the heat transfer coefficient range from 704 to 1,961 W/(m² K) on the condition of lumen-side feed, which was larger than that of shell-side feed operations (425–645 W/(m² K)). The results were inconsistent with the flux results (Fig. 3).

Table 3
Overall heat transfer coefficient of different module configurations

Module configurations	Overall heat transfer coefficient H ($W/(m^2 K)$)	
	Shell-side feed	Lumen-side feed
Randomly packed module	425	704
Curly fiber module	550	1,191
Spacer scattered module	562	1,333
Spacer knitted module	645	1,961

The TPC analysis of different modules is shown in Fig. 5. It can be seen that the TPC of each module on the condition of lumen-side feed was higher than that on the condition of shell-side feed. Lower TPC value means higher thermal boundary layer resistance and thus lower mass transfer coefficient and flux [21]. It can be concluded that the TP was more serious in the shell-side feed process, which was also confirmed by the flux (Fig. 3) and heat transfer coefficient results (Table 3). In this work, when the feed was pumped through the shell side, the feed velocity was lower, so the hot boundary layer became thicker and resulted in a relative low driving force and flux.

Compared with randomly packed module, the spacer knitted module shows the highest TPC (0.77–0.65 at $T_m = 303$ –313 K) followed by the spacer scattered (0.66–0.53 at $T_m = 303$ –313 K) and curly fiber modules (0.58–0.46 at $T_m = 303$ –313 K) (lumen-side feed). That might be due to the application of spacer and wavy geometries can facilitate a meandering fluid flow in the shell side, thereby achieved a well-mixed

condition and a mitigation of TP. And also from Fig. 5, it can be observed that the TPC decreased with T_m which might be due to higher fluxes generated by the higher vapor pressure gradient of dp/dT result in an increase in the effective membrane transfer coefficient h_m [12].

4.4. Residence time distribution (RTD) tests

Fig. 6 depicts the effluent tracer concentration of different modules as a function of time (first 30 s). The solid lines and dots are the experimental data, while the dots lines are the Gaussian distribution curves that have symmetric shapes to simplify the probability prediction. It can be seen from Fig. 6 that the RTD curves of the randomly packed module had relatively wider dispersions and double peaks that imply the existence of parallel flow paths or channeling in the modules. The curly fiber, spacer scattered and spacer knitted module showed narrower RTD curves compared with that of the randomly packed module, which showed a more ideal pattern of flow in the module.

The statistical parameter based on the RTD curves, the mean residence time t_m , and the dimensionless variance σ_m^2 , are summarized in Table 4. As seen in Table 4, the mean residence time of randomly packed module was 9.72 s, while that of curly fiber module, spacer scattered, and spacer knitted module were longer and to be 10.31, 10.45, and 10.62 s, respectively. The longer residence time indicates the longer contact time of fluid and membranes, which favors the mass and heat transfer during DCMO process [22].

The variance σ_m^2 is also an important metric to evaluate the flow distribution [12,24–26]. A smaller variance indicates a narrower RTD curve dispersion and a more ideal flow pattern [12]. As seen in Fig. 6, the $C(t)$ curve of curly fiber, spacer scattered and spacer knitted module shows a relatively spiked shape that indicates a reasonable uniform flow distribution which is consistent with their small variances (0.0148, 0.0137,

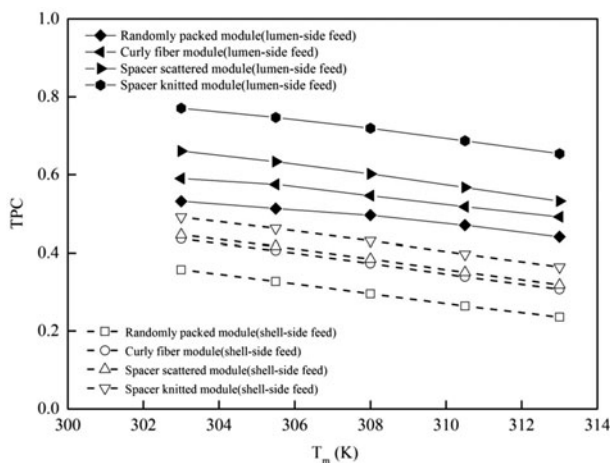


Fig. 5. Comparisons of the TP effect for various module configurations ($T_f = 308$ –328 K, $T_p = 298$ K, Q_f : 1.0–2.5 L/min; Q_p : 1.0 L/min).

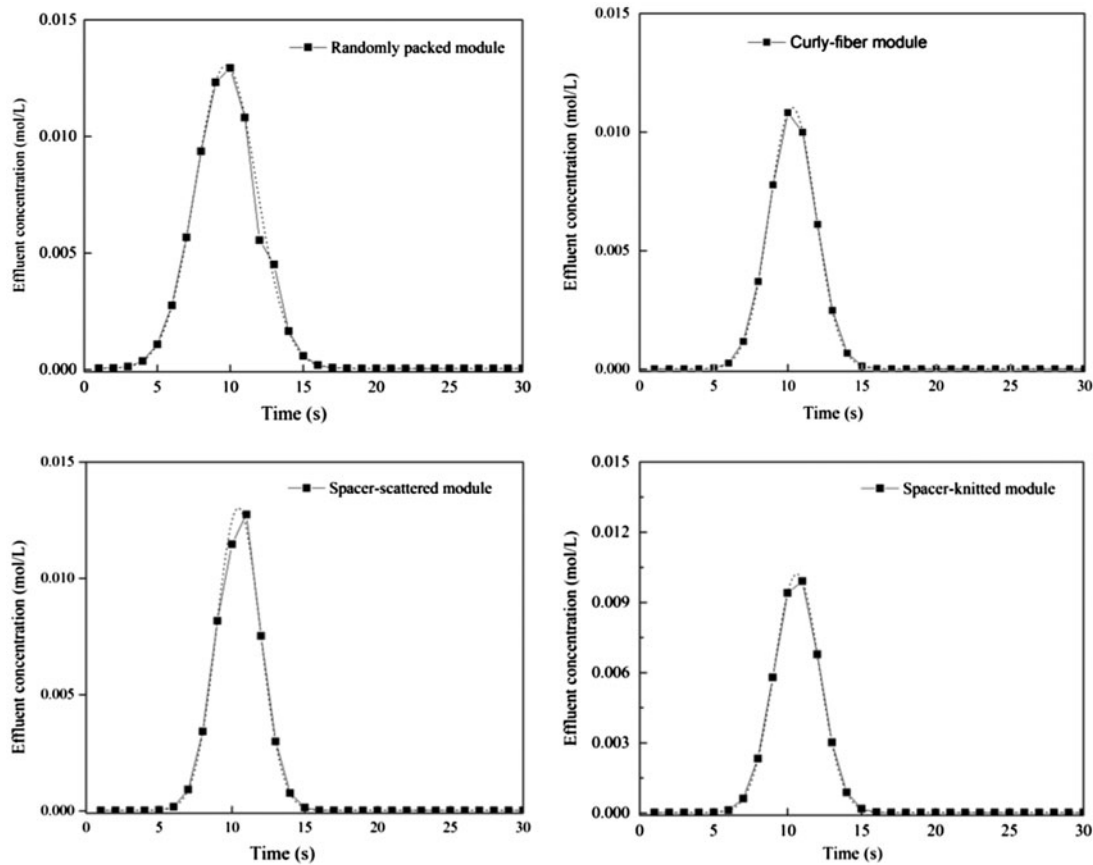


Fig. 6. Effluent tracer concentration of various configurations (tracer: sodium chloride solution; $Q_p = 1.0$ L/min, $T_p = 298$ K).

Table 4
Overall RTD results for various configurations

Configurations	Mean residence time t_m (s)	Variance σ_m^2 (dimensionless)
Randomly packed module	9.72	0.0222
Curly fiber module	10.31	0.0147
Spacer module	10.45	0.0137
Spacer knitted module	10.62	0.0135

0.0135). The RTD results were correlated with the module performance which confirmed that the modified module enabled more even flow distribution, and thus an enhanced mass and heat transfer coefficient.

5. Conclusions

In this study, hollow fiber membrane modules with spacer and curly geometries were designed. Their DCMD performance and heat transfer analysis on the condition of lumen-side feed and shell-side feed were

investigated compared with randomly packed module. In addition, the flow distribution in shell side was conducted. The main conclusions include:

- (1) The flux of lumen-side feed operation was higher than that of shell-side feed of different modules. Compared with randomly packed module, all the modified modules enabled higher permeate flux and the spacer knitted module has the best performance of 51.8% at 328 K in lumen-side feed performance.

- (2) Modified modules showed relative high flux even at a low feed flow rate, which confirms the fluid improvement caused by the spacers or wavy geometries.
- (3) Compared with randomly packed module, higher H and TPC were observed with modified modules due to a well-mixed condition caused by spacers and wavy fibers in the shell side, which was in accordance with the flux.
- (4) Longer residence time, smaller variances were found in modified module configurations based on RTD tests, which showed a more ideal flow pattern in modified modules.

Above all, theoretically lumen-side feed is recommended in DCMD process due to its high thermal efficiency. Proper modification favors the mass and heat transfer due to the creation of meandering flow rate and mitigation of TP.

Acknowledgments

This work is sponsored by Fundamental Research Funds for the Central Universities (TD2011-24, TD-JC-2013-3), the Beijing Natural Science Foundation (8132040) and the Beijing Municipal Science and Technology Commission (Z14110000914002).

Nomenclature

N	— vapor flux (L/(m ² h))
A	— effective membrane area (m ²)
C	— mass transfer coefficient (kg/(m ² h kPa))
P	— saturated vapor pressure of the bulk streams (kPa)
T_f	— bulk temperature of the feed (K)
T_{fm}	— temperature at the membrane surface on the feed (K)
T_p	— bulk temperature of the permeate (K)
T_{pm}	— temperature at the membrane surface on the permeate (K)
T_m	— membrane temperature (K)
τ	— temperature polarization coefficient (dimensionless)
P	— vapor pressure (kPa)
λ	— latent heat of vaporization (kJ/kg)
R	— gas constant (8.314 J/(mol K))
M	— molecular weight of water (g/mol)
Q	— total heat flux (W/m ²)
q_f	— heat flux toward heat boundary layers (W/m ²)
q_p	— heat flux toward cold boundary layers (W/m ²)
q_m	— heat flux between the membrane (W/m ²)
q_c	— conductive heat loss through the membrane (W/m ²)
q_v	— latent heat flux (W/m ²)

h_f	— feed side local heat transfer coefficient (W/(m ² K))
h_p	— permeate side local heat transfer coefficient (W/(m ² K))
h_m	— transmembrane heat transfer coefficient (W/(m ² K))
H	— the overall heat transfer coefficient (W/(m ² K))
k_m	— thermal conductivity of membrane (W/(m K))
δ_m	— wall thickness of membrane (m)
ε	— the membrane porosity (%)
k_s	— thermal conductivities of solid (W/(m K))
k_v	— thermal conductivities of gases in the pores (W/(m K))
$E(t)$	— residence time distribution function
$C(t)$	— temporal tracer concentration at the effluent (mol/L)
t	— time (s)
t_m	— mean residence time (s)
V	— volume of the vessel (m ³)
Q_f	— feed flow rate (L/min)
Q_p	— permeate flow rate (L/min)
V_f	— recirculated feed velocity (m/s)
V_p	— recirculated permeate velocity (m/s)

References

- [1] K.W. Lawson, D.R. Lloyd, Membrane distillation, *J. Membr. Sci.* 124(1) (1997) 1–25.
- [2] E. Drioli, A. Ali, F. Macedonio, Membrane distillation: Recent developments and perspectives, *Desalination* 356 (2015) 56–84.
- [3] M.S. El-Bourawi, Z. Ding, R. Ma, M. Khayet, A framework for better understanding membrane distillation separation process, *J. Membr. Sci.* 285(1–2) (2006) 4–29.
- [4] H. Susanto, Towards practical implementations of membrane distillation, *Chem. Eng. Process.* 50 (2011) 56–88.
- [5] X. Yang, R. Wang, A.G. Fane, C.Y. Tang, I.G. Wenten, Membrane module design and dynamic shear-induced techniques to enhance liquid separation by hollow fiber modules: A review, *Desalin. Water Treat.* 51 (2013) 3604–3627.
- [6] A. Gabelman, S. Hwang, Hollow fiber membrane contactors, *J. Membr. Sci.* 159(1–2) (1999) 61–106.
- [7] D. Qu, J. Wang, D. Hou, Z. Luan, B. Fan, C. Zhao, Experimental study of arsenic removal by direct contact membrane distillation, *J. Hazard. Mater.* 163 (2009) 874–879.
- [8] D. Qu, J. Wang, L. Wang, D. Hou, Z. Luan, Integration of accelerated precipitation softening with membrane distillation for high-recovery desalination of primary reverse osmosis concentrate, *Sep. Purif. Technol.* 67 (2009) 21–25.
- [9] F. Macedonio, A. Ali, T. Poerio, E. El-Sayed, E. Drioli, M. Abdel-Jawad, Direct contact membrane distillation for treatment of oilfield produced water, *Sep. Purif. Technol.* 126 (2014) 69–81.

- [10] K.C. Wijekoon, F.I. Hai, J. Kang, W.E. Price, T.Y. Cath, L.D. Nghiem, Rejection and fate of trace organic compounds (TrOCs) during membrane distillation, *J. Membr. Sci.* 453 (2014) 636–642.
- [11] D. Qu, D. Sun, H. Wang, Y. Yun, Experimental study of ammonia removal from water by modified direct contact membrane distillation, *Desalination* 326 (2013) 135–140.
- [12] X. Yang, R. Wang, A.G. Fane, Novel designs for improving the performance of hollow fiber membrane distillation modules, *J. Membr. Sci.* 384 (2011) 52–62.
- [13] L. Cheng, P. Wu, J. Chen, Modeling and optimization of hollow fiber DCMD module for desalination, *J. Membr. Sci.* 318 (2008) 154–166.
- [14] L. Song, B. Li, K.K. Sirkar, J.L. Gilron, Direct contact membrane distillation-based desalination: Novel membranes, devices, larger-scale Studies, and a model, *Ind. Eng. Chem. Res.* 46 (2007) 2307–2323.
- [15] X. Yang, R. Wang, L. Shi, A.G. Fane, M. Debowski, Performance improvement of PVDF hollow fiber-based membrane distillation process, *J. Membr. Sci.* 369(1–2) (2011) 437–447.
- [16] K. Schneider, W. Hölz, R. Wollbeck, S. Ripperger, Membranes and modules for transmembrane distillation, *J. Membr. Sci.* 39(1) (1988) 25–42.
- [17] L. Martínez-Díez, M.I. Vázquez-González, F.J. Florido-Díaz, Study of membrane distillation using channel spacers, *J. Membr. Sci.* 144(1–2) (1998) 45–56.
- [18] M.M. Teoh, S. Bonyadi, T.S. Chung, Investigation of different hollow fiber module designs for flux enhancement in the membrane distillation process, *J. Membr. Sci.* 311(1–2) (2008) 371–379.
- [19] X. Yang, E.O. Fridjonsson, M.L. Johns, R. Wang, A.G. Fane, A non-invasive study of flow dynamics in membrane distillation hollow fiber modules using low-field nuclear magnetic resonance imaging (MRI), *J. Membr. Sci.* 451 (2014) 46–54.
- [20] R.W. Schofield, A.G. Fane, C.J. Fell, Heat and mass transfer in membrane distillation, *J. Membr. Sci.* 33 (1987) 299–313.
- [21] T.K. Sherwood, R.L. Pigford, C.R. Wilke, *Mass Transfer*, McGraw-Hill, New York, NY, 1975.
- [22] O. Levenspiel, *Chemical Reaction Engineering*, third ed., John Wiley & Sons, New York, NY, 1999, pp. 260–265.
- [23] S. Bouguccha, R. Chouilkh, M. Dhahbi, Numerical study of the coupled heat and mass transfer in membrane distillation, *Desalination* 152 (2002) 245–252.
- [24] T.J. Rector, J.L. Garland, S.O. Starr, Dispersion characteristics of a rotating hollow fiber membrane bioreactor: Effects of module packing density and rotational frequency, *J. Membr. Sci.* 278 (2006) 144–150.
- [25] V. Dindore, A. Cents, D. Brillman, G. Versteeg, Shell-side dispersion coefficients in a rectangular cross-flow hollow fibre membrane module, *Chem. Eng. Res. Des.* 83 (2005) 317–325.
- [26] M.W.D. Brannock, Y. Wang, G. Leslie, Evaluation of full-scale membrane bioreactor mixing performance and the effect of membrane configuration, *J. Membr. Sci.* 350(1–2) (2010) 101–108.